International Journal of Fatigue 97 (2017) 29–38

Contents lists available at ScienceDirect

International Journal of Fatigue

journal homepage: www.elsevier.com/locate/ijfatigue

Propagation of surface initiated rolling contact fatigue cracks in bearing steel

Pawel Rycerz, Andrew Olver, Amir Kadiric *

Tribology Group, Department of Mechanical Engineering, Imperial College London, UK

ARTICLE INFO

Article history:
Received 3 August 2016
Received in revised form 30 November 2016
Accepted 2 December 2016
Available online 5 December 2016

Keywords:
Rolling contact fatigue
Pitting
Crack propagation
Rolling bearings
Flaking

ABSTRACT

Surface initiated rolling contact fatigue, leading to a surface failure known as pitting, is a life limiting failure mode in many modern machine elements, particularly rolling element bearings. Most research on rolling contact fatigue considers total life to pitting. Instead, this work studies the growth of rolling contact fatigue cracks before they develop into surface pits in an attempt to better understand crack propagation mechanisms. A triple-contact disc machine was used to perform pitting experiments on bearing steel samples under closely controlled contact conditions in mixed lubrication regime. Crack growth across the specimen surface was monitored and crack propagation rates extracted. The morphology of the generated cracks was observed by preparing sections of cracked specimens at the end of the test. It was found that crack initiation occurred very early in total life, which was attributed to high asperity stresses due to mixed lubrication regime. Total life to pitting was dominated by crack propagation. Results provide direct evidence of two distinct stages of crack growth in rolling contact fatigue: stage 1, within which cracks grow at a slow and relatively steady rate, consumed most of the total life; and stage 2, reached at a critical crack length, within which the propagation rate rapidly increases. Contact pressure and crack size were shown to be the main parameters controlling the propagation rate. Results show that crack propagation under rolling contact fatigue follows similar trends to those known to occur in classical fatigue. A log-log plot of measured crack growth rates against the product of maximum contact pressure and the square root of crack length, a parameter describing the applied stress intensity, produces a straight line for stage 2 propagation. This provides the first evidence that growth of hereby-identified stage 2 rolling contact fatigue cracks can be described by a Paris-type power law, where the rate of crack growth across the surface is proportional to the contact pressure raised to a power of approximately 7.5.

1. Introduction

The subject of this paper is the propagation of surface initiated rolling contact fatigue (RCF) cracks, which leads to the mode of contact failure known as pitting, characterised by a loss of material from the load-bearing surface in form of crater-shaped cavities or pits. Provided that running conditions are sufficiently good to eliminate premature failure by all other mechanisms, pitting ultimately limits the life of machine components subjected to concentrated rolling/sliding contacts such as rolling element bearings, gears and cam/follower systems [1]. The process of pitting failure involves the initiation of micro-cracks within the stressed volume via a damage accumulation process, subsequently followed by their growth, which eventually leads to the generation of surface pits and the ultimate failure of the component.

Pitting failures are often categorised by the location of incipient cracks; subsurface-initiated pitting is caused by crack initiation at or near inclusions in the sub-surface zone affected by contact stresses, while surface-initiated pitting begins with crack initiation either at indigenous stress raisers present on the surface of the material, such as scratches, grinding furrows and near-surface inclusions, or defects introduced during operation, for example debris indentations or damage arising from asperity contact [2–4].

In modern bearings, the frequency of subsurface initiated failures has been significantly reduced from the levels seen in the past, primarily owing to improvements in steelmaking, resulting in much cleaner steels with lower inclusion content. In contrast, the incidence of surface-initiated failures has grown in modern machines, not least due to the fact that machine efficiency improvements are often sought through a reduction in lubricant viscosity and

* Corresponding author.
E-mail address: a.kadiric@imperial.ac.uk (A. Kadiric).

http://dx.doi.org/10.1016/j.ijfatigue.2016.12.004
0142-1123/

increase in power density. Resulting low specific film thickness means that components often operate in severe lubrication conditions increasing the probability of surface initiated failures. This work investigates surface initiated pitting failures under mixed lubrication regime pertinent to failures observed in the field in modern rolling element bearings.

Since the pioneering work of Way [5] surface initiated pitting has been the subject of extensive research, focused mainly on the determination of factors influencing life. A number of previous works highlighted the influence of specific film thickness and surface roughness on life [2,6–14]. Other authors showed that surface traction and its direction was significant [2,15,16]. In terms of damage morphology, it was generally found that surface cracks initially grow at shallow angles (~30°) to the surface, their orientation controlled by the direction of the applied traction force [2,15,16]. Once they reach larger depths, cracks turn from their initial angle of propagation to grow parallel to the surface [15,17]. At the surface, cracks display a characteristic V-shape, often referred to as 'fan' shape. Pits are usually formed when a secondary crack branches out and breaks the surface [15,17].

The majority of past experimental work was conducted using the 'total life' methodology, whereby the life to failure is measured under various operating conditions. This approach, combined with a statistical treatment of failure rates, allowed the formulation of bearing life rating models [18–20], however the fundamentals of crack propagation under rolling contact remain relatively poorly understood.

A number of researchers applied theoretical linear elastic fracture mechanics (LEFM) methods to determine stress intensity factors (SIFs) for idealized crack geometries under rolling/sliding contact. In his early paper, Keer [21] showed that crack propagation occurred in pure shear mode when the influence of lubricant was not accounted for. Miller [22] found that asperity stresses were the dominant driver for the propagation of short, shallow cracks and bulk Hertzian stresses took over as cracks increased in size. Kaneta and Murakami [22–26] published a number of studies in which they analysed the propagation of surface cracks, with particular attention to the effects of fluid ingress. They proposed that short cracks propagated in shear mode at their initial angle and remained closed during passage of contact, precluding fluid ingress. Upon reaching a certain size, crack opening was enabled causing fluid ingress and inducing a large tensile stress at the crack tip via either hydraulic pressurization or fluid entrapment. This caused a change in the growth direction towards the surface, and possibly higher propagation rates. Bower [28] later concluded that the fluid entrapment conjecture was the most consistent with experimental observations while Hanson [29] also postulated that fluid pressure was necessary for propagation.

The theoretical LEFM work shed some light on potential propagation mechanisms and provided methods to calculate stress intensity factors for RCF cracks. Some authors used the results of their models in conjunction with Paris law for crack growth in an attempt to predict life to failure based on fracture mechanics [29]. This approach is commonly used in damage tolerant life rating methods in structural fatigue. However, in structural fatigue theoretical LEFM prediction methods are backed by a vast body of experimental work on crack growth in various materials and under various loading and environmental conditions.

In contrast, experimental data concerning rolling contact fatigue crack growth is scarce due to the inherent difficulties in measuring crack growth under rolling contact conditions. Nevertheless, a number of authors studied surface RCF cracks using disc machines and attempted to characterise the process of RCF crack growth. Soda et al. [2] found that propagation occurred in two regimes: shallow cracks propagated at a low rate which accelerated when they reached a certain size. Murakami et al. [30] and Tyfour et al. [31] found that reversing either the direction of rotation or the direction of the applied traction force resulted in crack growth arrest, confirming the possible influence of fluid on surface crack propagation.

Although qualitative observations of surface crack propagation were reported in a number of previous publications there is a lack of quantitative data in the form of crack propagation rates measured under various conditions. As a result, it remains unknown whether the LEFM methods employed in structural fatigue can be applied to rolling contact fatigue, despite the fact that the fundamental fatigue mechanisms may well be the same [15]. In order to bridge this knowledge gap, an improved understanding of rolling contact fatigue mechanisms is needed, starting with relevant experimental data on crack initiation and growth.

The present work aims to extend the knowledge in this area with particular focus on the propagation of surface initiated RCF cracks in bearing steel. Detailed observations of surface crack growth under rolling/sliding contact in steel bearing rollers were performed using a three-contact RCF test machine. The primary objectives of this study were:

- To study surface initiated rolling contact fatigue cracks, with realistic morphology representative of engineering components, and under controlled contact conditions
- To provide new quantitative data on crack propagation rates within a wide range of crack lengths and at different contact pressures
- To study the relative duration of crack initiation and propagation phases
- To assess the feasibility of using LEFM methods to predict rolling contact fatigue crack growth based on a suitable crack propagation law

2. Experimental methodology

2.1. Test rig description

Experiments were conducted using a PCS Instruments Micropitting Rig (MPR). The MPR is a rolling contact fatigue tester in which three counter-face discs of 54.15 mm diameter are loaded against a 12 mm diameter central roller specimen. Fig. 1a shows an overview of the MPR test chamber and loading system. Load is applied using a stepper motor driven ball-screw to the load beam, which transmits it to the specimens through the top counter-face disc. The system allows for the applied load to be controlled in the range of 0–2000 N. Fig. 1b shows the arrangement of test specimens inside the test chamber. The test roller is centrally located between three counter-face discs which are spaced 120° apart. This geometry results in equal reaction forces at each of the three points of contact between the roller and the discs. The discs and roller are driven by independent electric motors, allowing any desired slide roll ratio between 0% (pure rolling) and 200% (pure sliding) to be set. The specimen assembly is dip lubricated from a temperature controlled oil sump. The rig is fitted with a custom made magnetic crack sensor which enables early, short cracks to be automatically detected during the test.

2.2. Test specimens

The test specimens were cylindrical rollers made out of AISI 52100 steel. The rollers were taken directly out of a NU1018 bearing, ensuring that the material is representative of modern bearing steels, and had a slot machined at the back to provide drive in the test rig. The measured hardness and surface roughness were 756HV and 0.03 μm Ra respectively. The geometry of the roller specimen is illustrated in the drawing in Fig. 2. Two types of

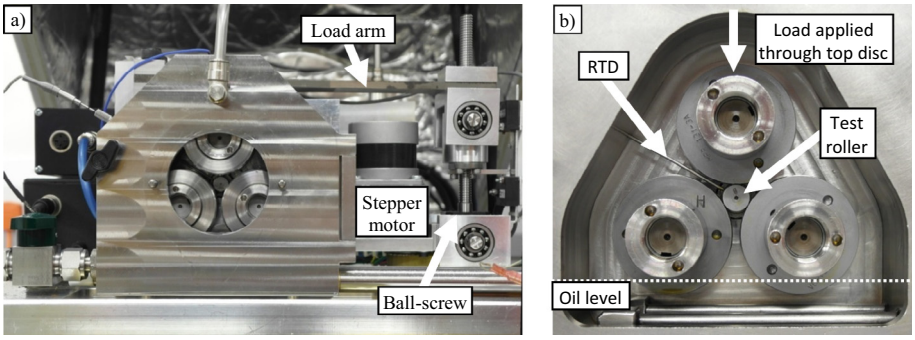

Fig. 1. (a) Micropitting test rig chamber and loading system (b) Specimen configuration inside the test chamber.

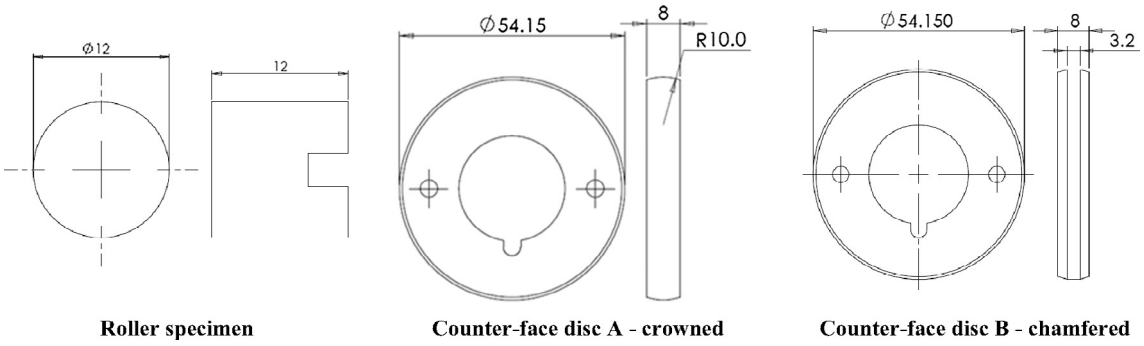

Fig. 2. Test specimen geometry.

Table 1
Specimen material and surface roughness parameters.

	Material	Hardness (HV)	Surface roughness Ra (μm)
Roller specimen	AISI 52100	756	0.03
Counterface disc A	AISI 52100	789	0.15
Counterface disc B	AISI 52100	784	0.15

Table 2
General test conditions.

Entrainment speed	3.8 m/s
Slide/roll ratio	5% (roller specimen slower)
Lubricant	PAO + ZDDP (0.1%wt P)
Lubricant viscosity	25 cSt at 40 °C 5 cSt at 100 °C
Lubricant sump temperature	65 ± 2 °C
Estimated minimum film thickness	~60 nm
Initial lambda ratio (=minimum film thickness/compound Ra roughness)	~0.26

PAO – polyalphaolefin lubricant base stock.
ZDDP – zincdialkyl-dithiophosphate anti-wear additive.

counter-face discs were used in the present study: crowned (A) and chamfered (B). The geometries of both are shown in Fig. 2. The discs are made out of AISI 52100 steel, hardened to 780–790 HV and finished to 0.15 μm Ra as listed in Table 1. The roughness lay on both the roller specimens and the counterface discs is circumferential i.e. parallel to the rolling direction. Roughness of all specimens was measured prior to each test to ensure consistency, and a new set or counter-face discs was used in each test.

2.3. Test conditions

General test conditions are outlined it Table 2. All tests were run at an entrainment speed $[(U_{disc} + U_{roller})/2]$ of 3.8 m/s and with a slide-roll ratio of 0.05 between the roller and disc surfaces in order to simulate the low level of sliding occurring in rolling element bearings. Here the slide-roll ratio is defined as $[(U_{disc} - U_{roller})/U_{entrainment}]$. In order to localize the damage on the roller specimen the slide-roll ratio was set to be positive i.e. the roller surface velocity was lower than that of the disc i.e. the roller was the 'follower'. The specimens were lubricated with a model oil made up of polyalphaolefin (PAO) base stock with only zincdialkyl-dithiophosphate (ZDDP) anti-wear additive added at a concentration of 0.1% wt phosphorus. The use of a simple model lubricant with known properties, rather than a commercial oil, ensures that any influences of a complex, and usually unknown, commercial lubricant formulation are excluded. The ZDDP was added in order to ensure that no appreciable wear occurred during testing. This ensured that competition between surface wear and crack initiation/propagation did not affect crack measurements, as well as preserving the geometry of the specimens so that the contact pressure remained constant throughout the tests. The lubricant had a measured viscosity of 25 cSt at 40 °C and 5 cSt at 100 °C. The base stock of this particular low viscosity was selected in order to ensure that the contact operated in mixed lubrication conditions, which helps promote surface crack initiation as necessary for this study. The lubricant sump was kept at a constant temperature of 65 ± 2 °C. The elastohydrodynamic lubricant film thickness, estimated using the Hamrock-Dowson equation, was 60 nm. Therefore, the initial Λ ratio, defined as the minimum film thickness divided by compound specimen Ra roughness, was about 0.26.

2.4. Test procedure

The test procedure was designed to generate surface initiated RCF cracks, detect them in early stages of life and measure their growth rates *across the surface*. Measuring RCF crack propagation rates requires a method to detect early surface cracks *in situ* during a test. In order to achieve that, a crack sensor based on the principle of magnetic flux leakage [32] was developed and installed on the test rig. The sensor continuously scans the roller specimen surface and automatically halts the machine when a crack is found. The present setup enables crack detection in specimens without any pre-installed defects, i.e. without knowing the location of the initiation site a priori.

The aim of this study was to track surface crack growth over a number of contact cycles for a given surface initiated rolling contact fatigue crack. To achieve this a non-destructive procedure had to be adopted. To start with, pitting tests were run until cracks initiated in the roller specimens. In order to accelerate crack initiation, this phase was run at a relatively high maximum Hertzian contact pressure of 4.76 GPa using counter-face disc A (test condition 1). Upon crack detection, tests were interrupted and roller specimens taken out for inspection. Photographs of cracks were taken using an optical microscope. Specimens were then returned to the test rig for the next part of the test during which cracks were grown in a controlled manner. Tests were restarted for a predetermined number of cycles, after which specimens were inspected again and new photographs of the followed surface cracks taken. This procedure was repeated until pitting occurred or until a crack of a desired length was produced.

Type A crowned discs were used to obtain relatively high contact pressures of 3.63 GPa and 4.76 GPa. In order to be able to study the behaviour of relatively long cracks, with surface lengths longer than the maximum transverse contact width achievable with crowned discs, type B chamfered discs were employed to increase the contact width and hence propagate the cracks further; in this case the contact pressures were 2.15 and 1.73 GPa. All test conditions used are summarised in Table 3 and the contact geometries achieved with the two types of discs are shown in Fig. 3. For high-pressure, elliptical cases more than 6 separate tests (different set of specimens each time) were performed and in all cases multiple cracks were followed on any single roller specimen. In total more than 20 cracks in this configuration were studied. For the low-pressure, line contact cases, one set of tests was performed at each of the two pressures with a single crack followed in each test.

Data for crack growth across the surface was obtained from the sequences of photomicrographs of surface cracks taken throughout the test as explained above. Subsequent images of cracks were overlaid, as shown in Fig. 4, and a line was fitted to the newly grown portion of the crack. This line enabled the measurement of the crack extension over the given number of cycles corresponding to the two images. Where crack extension rate per contact cycle, dc/dN, was needed, this was obtained by dividing the crack extension result by the number of cycles in each step. It is important to note that in all cases, the crack lengths quoted correspond to the length of the crack on the surface only. It is not possible to obtain measurements of subsurface crack growth progression for a given crack in this type of rolling contact.

3. Results

3.1. Observed crack morphology

The micrographs in Fig. 5 show examples of typical early surface initiated cracks found on the roller specimen. The smallest measured crack had a surface length of ~20 μm. Despite their short length of below 50 μm, the early cracks already display a fully developed, characteristic 'fan' shape, indicating that at this length they have already undergone some amount of propagation, thus suggesting that their size at initiation was much smaller. In terms of initiation sites, most early cracks occurred in apparently defect-free locations on the surface, with only some of them being visibly associated with voids or micro-pits.

The test procedure employed in this study, described above, enabled tracking of crack growth starting at a very early stage until the formation of a spall; an example of this is shown in Fig. 6. Typical patterns of crack propagation across the surface that were recorded are illustrated by the sequences of optical micrographs in Figs. 7 and 8, which show crack propagation under elliptical and line contact respectively. It was observed that cracks grew in the direction of contact patch motion (i.e. against the rolling direction) and against the direction in which the friction force was acting. Upon reaching a certain crack length, the process of pit formation started with secondary cracks breaking the surface as seen in the final images of Figs. 7 and 8. Typically, this occurred when cracks extended enough to span the whole width of the running track (contact width in the transverse direction), at which point cracks ceased to grow in the transverse direction as the contact pressure drops to zero outside the running track, unless the specimen configuration is changed as to increase the width of the contact.

Metallographic sections were prepared in order to examine sub-surface crack morphology. Fig. 9 shows an example section of a large crack where the plane of the section is parallel to the rolling direction and passes through the middle of the crack in transverse direction. It can be seen that overall the crack propagated into the material at an angle to the surface. However, the crack path contains numerous points at which the direction of propagation changes locally. A higher magnification image of the same section is shown in Fig. 10, which more clearly illustrates the existence of kinks in the crack path and crack branching at these kinks. In addition, it can be seen that a significant amount of loose particles is present between the crack faces, probably indicative of crack faces rubbing against each other during contact passage.

The eventual pitting failure was generally observed to be preceded by secondary cracks appearing at the surface. Fig. 11 shows a transverse section of a crack illustrating this phenomenon: Secondary cracks are seen to branch off the main crack and grow towards the surface, eventually liberating a fragment of the material and starting pit formation.

Table 3
Contact conditions.

Test condition	Disc type	Load (N)	Maximum Hertz contact pressure, p_0 (GPa)	Contact width in rolling direction, b (μm)	Contact width transverse to rolling, a (μm)	Measured friction coefficient
1	A	2000	4.76 GPa	351	571	0.061
2	A	890	3.63 GPa	268	436	0.058
3	B	2000	2.15 GPa	185	1600	0.067
4	B	1300	1.73 GPa	149	1600	0.065

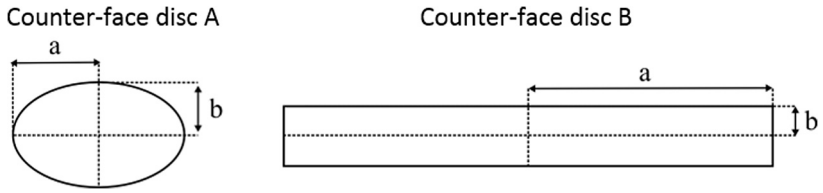

Fig. 3. Contact geometry with counter-face discs A and B. Rolling direction top to bottom.

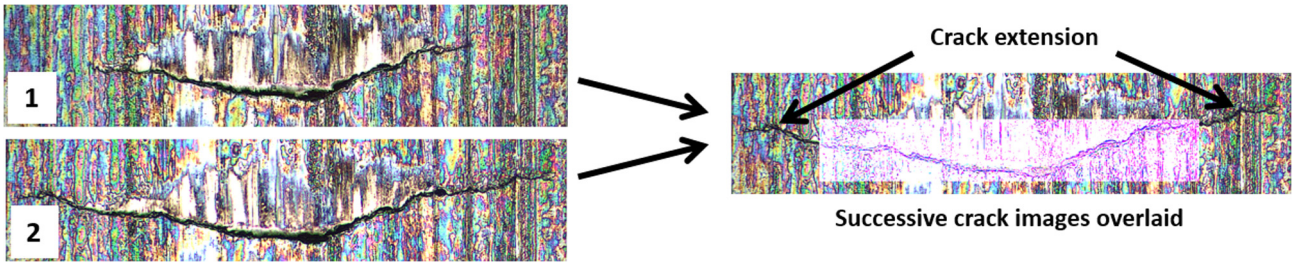

Fig. 4. Measurement of crack extension from optical micrographs.

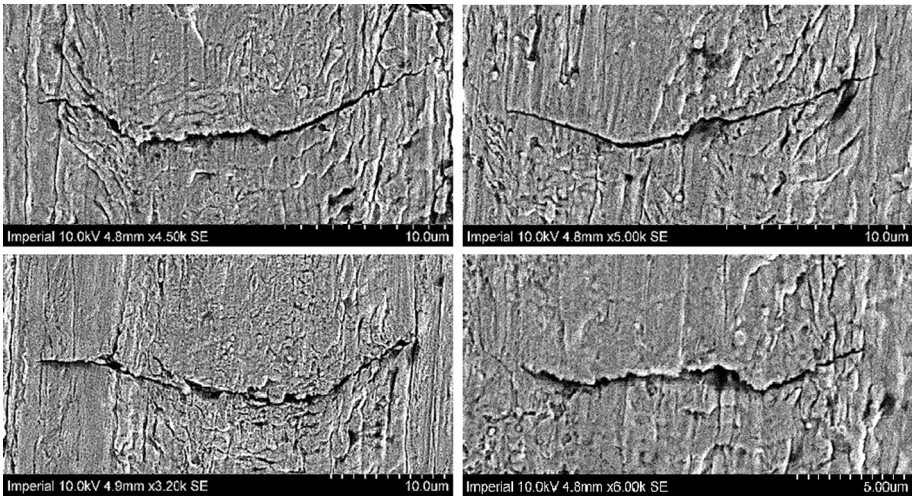

Fig. 5. SEM images of typical early surface cracks observed in this study.

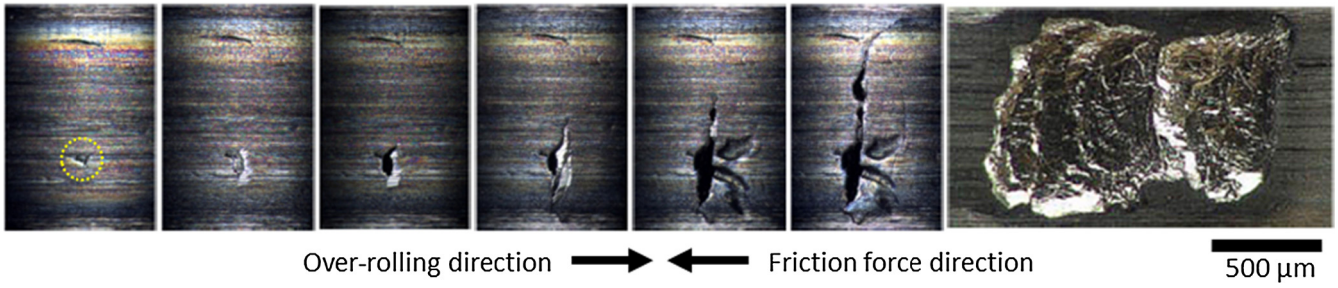

Fig. 6. An example of surface crack growth leading to pitting under test condition 1.

3.2. Crack growth rates

Fig. 12 shows a plot of surface crack growth rates as a function of crack length measured at various contact pressures, under elliptical and line contact geometries, type A and type B discs respectively. In case of elliptical contacts, this figure shows results from multiple different tests and more than 20 different cracks. The fact that they all follow the same general trend illustrates that the observed crack behaviour is consistent between different tests and cracks. It is apparent that, other than for very short cracks (p_0 = 4.76 GPa data), crack growth rate generally increases with crack length, with the rate of increase higher under elliptical contact. It is also evident that the effect of contact pressure was to increase the propagation rate regardless of contact geometry.

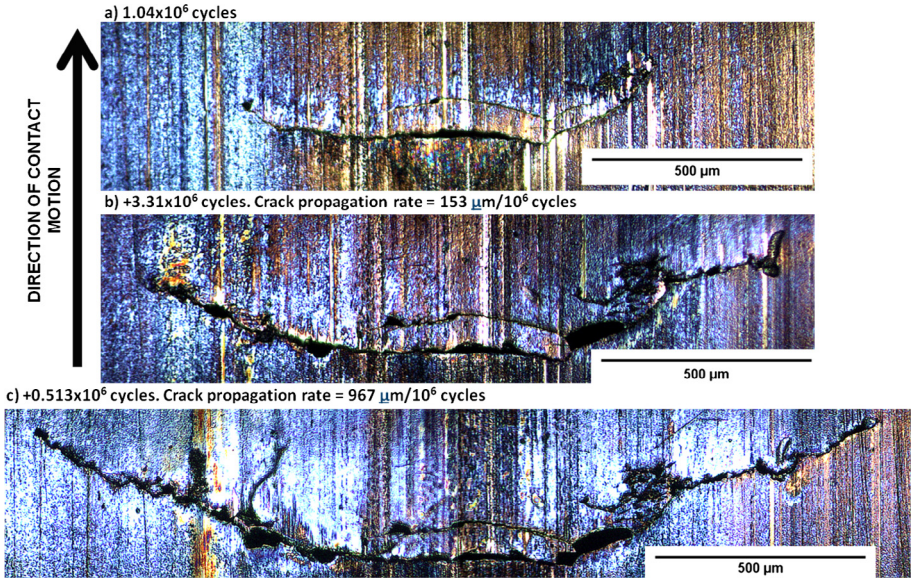

Fig. 7. Example of surface crack propagation under test condition 1.

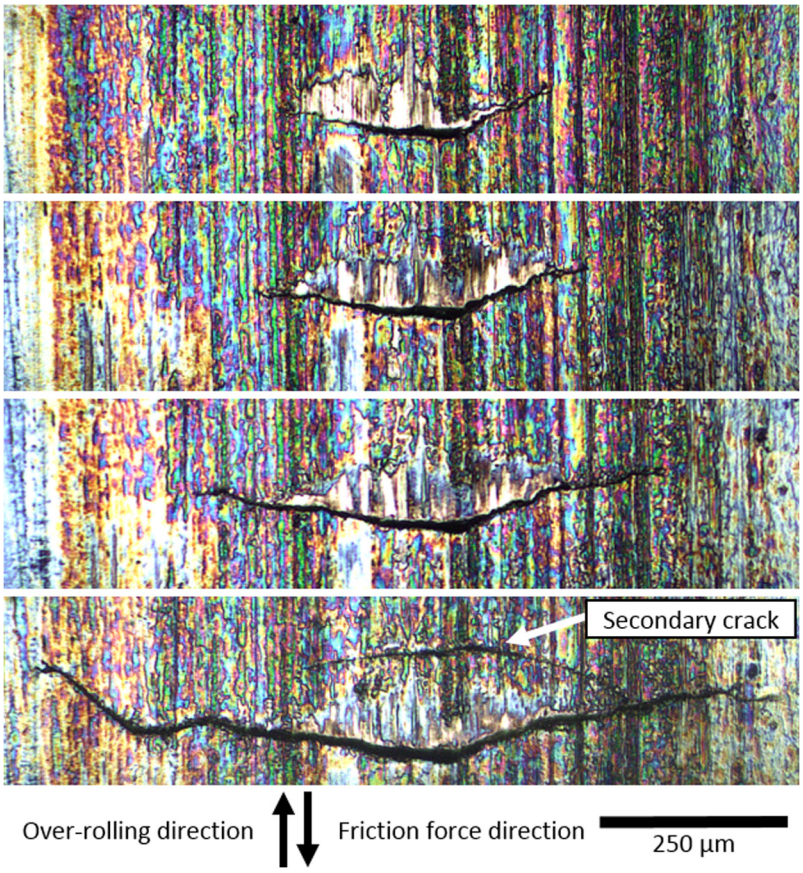

Fig. 8. Example of surface crack propagation under test condition 4.

3.3. Observed stages of crack growth

Fig. 13 shows the relationship between crack length and life to pitting from a series of experiments. In order to generalize and compare the results between the different tests, life is normalised by the total number of cycles at which pitting occurred in each test. The measurements were performed for 12 individual cracks, on four different roller specimens, propagated at the same maximum contact pressure of 4.76 GPa. Each of the curves in the graph represents an individual crack. It should be noted that some cracks may be from the same specimen e.g. the most left points on the graph, hence the same first normalised life values at this point.

It is apparent that for all cracks that were detected very early in their life, the life to first crack detection, by which time the cracks

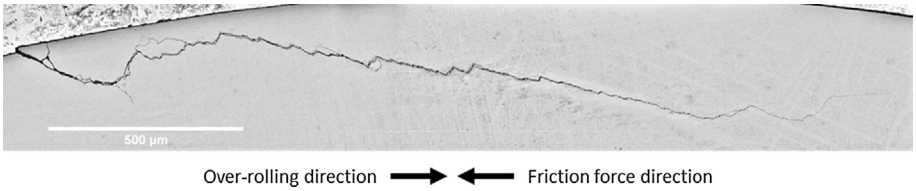

Fig. 9. A section parallel to rolling direction through the centre of a typical relatively long crack.

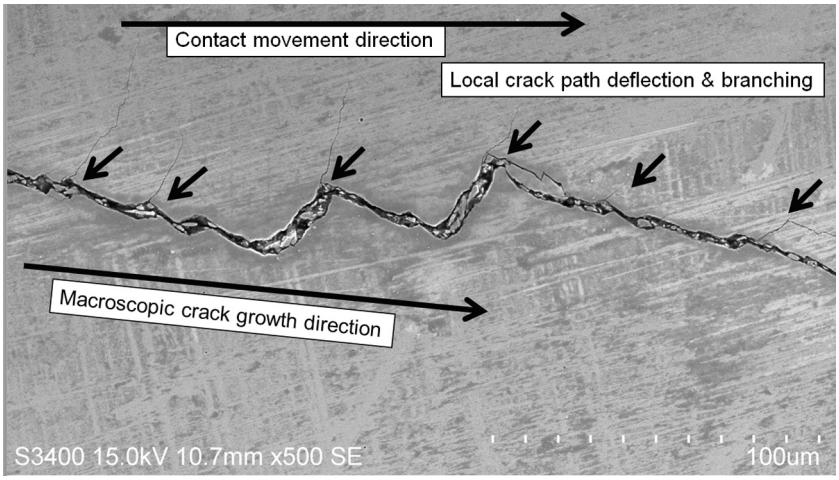

Fig. 10. Scanning electron microscope image showing detail of the sub-surface propagation trajectory of the crack in Fig. 9. Regular steps can be seen with secondary cracks at the corners. Apparent debris is also seen inside the crack.

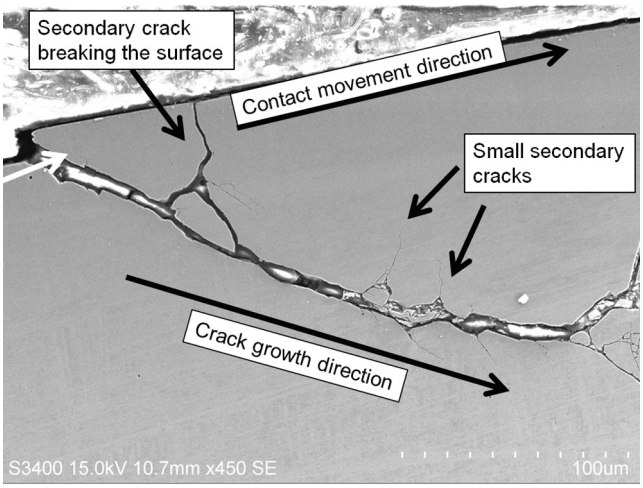

Fig. 11. Scanning electron microscope image showing detail of the mouth area of the crack in Fig. 9. Secondary cracks can be seen to branch off the main crack.

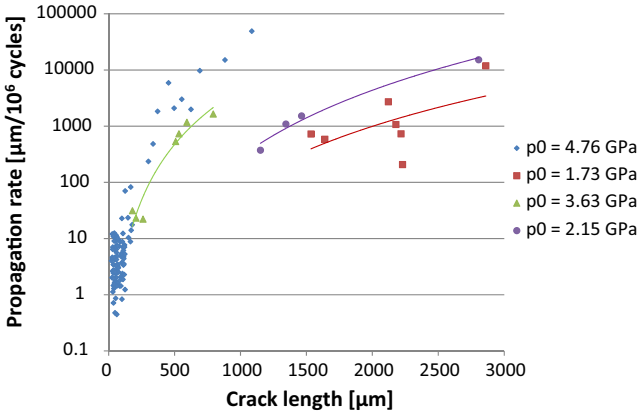

Fig. 12. Crack propagation rates as a function of contact pressure and contact geometry (4.76 and 3.63 GPa – elliptical contact, type A disc; 1.73 and 2.15 GPa - line contact, type B discs).

were already 20–60 µm in length, constituted only about 15% of the total life to pitting and that most of the life was consumed by the subsequent propagation phase. The precise length of time to the actual crack initiation itself is unknown. In fact, even if cracks could be detected at an earlier stage, defining initiation life exactly would be difficult since one would need to define some crack length to correspond to initiation. However, based on their already well-developed characteristic V-shape, it is reasonable to assume that the earliest cracks observed here had already undergone some propagation before they were detected. This means that the life to crack initiation is likely significantly shorter than the life to first detection quoted here, i.e. crack initiation might have occurred in the very early stages of the total life shown. It should be noted that the relative life proportion consumed by initiation and propagation in the current experiments is influenced by the imposed test conditions of very low specific film thickness, which favours early crack initiation; under better lubrication conditions the relative duration of initiation and propagation phases may be different.

Fig. 14 plots the crack propagation rates (dc/dN) against the instantaneous crack length, *c*, for the same individual cracks.

The results depicted in Figs. 13 and 14 show that following the first detection, the observed crack propagation phase can be split into two distinct stages:

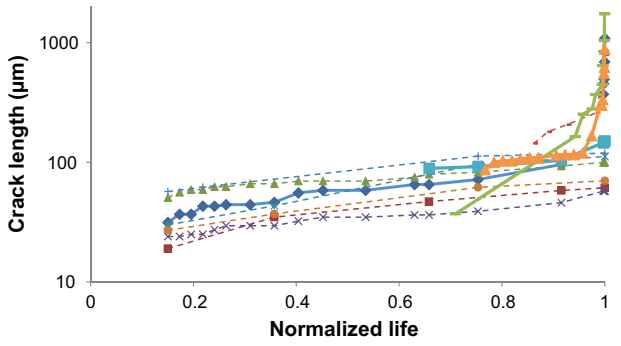

Fig. 13. Crack length as a function of cycle number normalised by the total number of cycles to failure for 12 individual cracks; Results for 4.76 GPa, elliptical contact, type A disc.

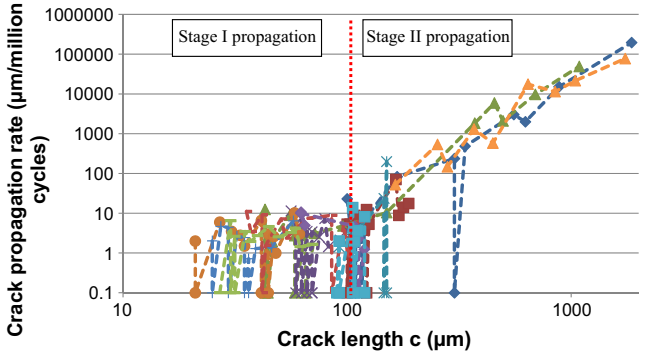

Fig. 14. Crack propagation rate across the surface *(dc/dN)* as a function of instantaneous surface crack length *(c)*; Results for 4.76 GPa, elliptical contact, type A disc.

I. *Stage 1 propagation:* Within this stage, applicable to small cracks, from about 20 to 100 μm in length, the propagation rates were relatively slow at ~0–10 μm per million contact cycles, and frequent periods of crack arrest (zero rate of propagation) occurred, as apparent in Fig. 14. Potential reasons for crack arrest are discussed later in the paper. The averaged propagation rates appeared to show a slight decrease as crack length increased within this region. In terms of fraction of the total life to pitting, this stage of crack growth was the most dominant, consuming about 70% of the total pitting life.

II. *Stage 2 propagation:* This stage, which covers cracks from about 100 μm onwards in length, is characterised by a marked increase in the speed of crack growth. In sharp contrast with stage I propagation, stage II growth rate increased rapidly with increasing crack size. This phase consumed the remaining ~15% of total life to pitting. In the final stages just prior to the formation of a pit very large growth rates of approximately 50,000 μm per million cycles were recorded.

4. Discussion

4.1. Observed crack morphology

Qualitative characterisation of crack behaviour observed in the present work reveals the following similarities with behaviour of rolling contact fatigue cracks observed in practical applications:

- Cracks display a v-shaped propagation pattern when viewed at the surface.
- Crack growth occurs in the direction opposite to the direction of the applied friction force i.e. against the rolling direction in the current set-up where the roller is slower than counterface.
- In parallel section view cracks have an initial angle of inclination to the surface of 20–30°.
- Secondary cracks form and grow to break the surface, eventually causing a pit to form.

In view of these observations, it can be concluded that the failure mode observed in the present study is representative of the generally accepted mechanisms of surface initiated rolling contact fatigue.

Further significant features of crack behaviour are evident in photographs of the sectioned cracked specimens shown in Figs. 9–11.

First of these is the evidence of crack branching, most apparent in Figs. 10 and 11. Crack branching has been associated with rolling contact fatigue cracks, not only in rolling bearings but also in rails [33], and it has been previously attributed to the mixed-mode loading conditions prevalent under rolling contact [27,32]. The existence of branching cracks in the present experiments might suggest that propagation indeed proceeded in mixed-mode with large mode II displacement. Bower [28] attaches particular importance to the propagation of branching cracks since they can start the process of pitting by reaching the surface. Such occurrence and growth of secondary branching cracks as a potential mechanism of pitting is supported by the present study, where secondary cracks have been observed to propagate to the surface, liberating a fragment of the material, as clearly evident in Fig. 11.

Second significant feature of cracks observed in this study is the existence of regular steps in the crack path, most evident in the close up of Fig. 10. This is a feature often associated with crack advance in mixed-mode [34] and it has been suggested that this type of morphology can significantly lower the stress intensity factors at the crack tip, due to inter-locking and rubbing between the fracture surfaces, especially when significant mode II displacements are present [34]. Potential for occurrence of crack rubbing under rolling contact conditions is seemingly supported in the present experiments by the presence of debris particles within the crack, which can be formed if locked crack faces undergo significant relative displacement during the passage of contact load. However, before concrete conclusions can be drawn in this respect, the possibility that the observed crack debris is simply an artefact of the sample preparation procedure must first be excluded. In addition to the apparent kinks in the crack path direction, the results presented here also show periods of crack arrest during the stage 1 propagation phase identified above. Perhaps the most obvious potential reason for this behaviour is the possible influence of microstructure, where individual grains present in the complex polycrystalline steel microstructure affect the crack growth rates and direction. Suresh et al. [35], amongst others, links the frequent deceleration and periods without propagation, as observed here (Fig. 14), to the sensitivity of crack growth rate to the crystallographic texture of the material and crack arrest at grain boundaries. The existence of prior austenite grain boundaries has been suggested to be particularly significant in this respect. Lankford [36] studied the growth of short cracks in a martensitic high strength steel and proposed that crack arrest occurred at prior-austenite grains. The AISI 52100 steel used in the present study has a comparable microstructure, therefore it is feasible that a similar mechanism was operative in present experiments. However, direct evidence of crack arrest at grain boundaries is very difficult to obtain in martensitic steels due to their very fine and complex microstructures. Indeed, Lankford did not observe interactions of the crack with grain boundaries directly but arrived at his conclusion by relating the length of propagation between

periods of stoppage to the average size of prior- austenite grains. In AISI 52100, the prior austenite-grain size depends on the heat treatment; in the steel used in the present study it is about 20–30 μm. Given the appearance of crack sections and measured propagation rates, it is possible that the presently observed crack arrests and deflections are indeed related to the microstructure but this should ideally be confirmed by direct observation.

As evident in Fig. 13, crack propagation phase consumes majority of the overall life under the conditions employed here, while crack initiation occurs relatively quickly. It is not possible to quantify the exact time to first initiation since surface cracks can only be detected once they are already a few tens of microns long, but based on the observations presented here, it can be said that crack initiation consumes less than 15% of the overall life. Here, it is perhaps worth considering previously published work on this subject, which at first sight may appear to contradict this observation. For example, Yoshioka and co-workers [37–39] use acoustic emission signals to monitor surface damage propagation under rolling contact fatigue and suggest that the crack initiation phase dominates life while propagation phase is very short. Although the possibility that the reported differences are due to different contact conditions employed cannot be ruled out, perhaps a more plausible explanation may lie in the fact that, relative to the present work, Yoshioka and co-workers only identified surface cracks at a very advanced stage of propagation, with the shortest reported cracks being in the range of 1 mm. This is much longer than the shortest observed cracks in the present work, which are of the order of tens of microns. At 1 mm in length, the cracks are already at an advanced stage of propagation, so that effectively most of the slow propagation phase, whose existence is identified in the present work, has already been consumed but missed by the detection technique they employ. Indeed, in the present experiments the propagation life from a crack length of 1 mm to eventual pitting also consumes a relatively small proportion of life. Therefore, although on first sight the two sets of results may appear contradictory, it is likely that they are in agreement and that the apparent differences arise from the different stages at which the cracks were first observed.

4.2. Observed crack behaviour in relation to classical fatigue

In classical tensile fatigue of high-strength steels, the propagation of stage 2 cracks generally follows the Paris law [Paris/Coffin/Manson]:

$$\frac{\mathrm{d}\,c}{\mathrm{d}\,N} = C\Delta K_{\mathrm{I}}^{m}$$

where ΔK_{I} is the range of stress intensity factor, c is the crack length, N is the number of cycles and C and m are constants. In seeking a similar correlation for rolling fatigue, we may reflect that:

(a) Owing to the complexity of the applied stress field, the effects of crack closure, lubrication and friction, there is no simple or unequivocal way to calculate K_{I}. Further difficulties arise where there is evidence (as here) of changes in the shape of the crack as it grows and of multiple and branched cracking.

(b) However, we might expect all the relevant stresses to scale to the maximum Hertz pressure p_0. If, in addition, the crack is small, compared to the dimensions of the volume affected by contact stresses, close to the area of contact, the range of stresses near the tip of the crack during over-rolling may be proportional to the parameter $p_0\, c^{1/2}$.

(c) If the crack grows to be significantly larger than the area of contact ($c > a, b$) or if its shape changes, we might expect this proportionality to become invalid.

In Fig. 15, crack growth rate is plotted against $p_0\, c^{1/2}$ for 22 cracks of lengths between ~20 and 2860 μm at various levels of contact pressure. The solid trend lines are fitted to individual crack data in the stage 1 propagation phase identified earlier and the single dashed trend line is fitted to all data in the stage 2 regime.

Plotted using logarithmic scales, the data in stage 2 crack growth regime falls on a straight line. This suggests that the crack growth response to the applied stress intensity in stage 2 can be described by a Paris-type power law. There does not seem to be any evidence of a reduction in crack growth rate below the trend for the larger cracks, so assumption (b) seems to be correct. The trend also suggests that the effective shape of the crack (only evident on the surface as a shallow "V") does not change significantly during stage 2 growth. The equation of the trend line fitted to the stage 2 crack growth data is:

$$\frac{\mathrm{d}\,c}{\mathrm{d}\,N} = 5\times 10^{-12}\ \mathrm{m}\left(\frac{p_0 c^{1/2}}{\mathrm{MPa\,m^{1/2}}}\right)^{7.5}$$

The constants C and m seem large compared to Paris law constants in classical fatigue but this is to be expected since, here, the majority of the stresses are *compressive* so that ΔK_I is perhaps a small, albeit roughly constant, proportion of $p_0\, c^{1/2}$.

In contrast, for stage 1, the rate of propagation *declines* with increasing stress intensity. Again this is strongly reminiscent of small crack behaviour in classical fatigue [40]. In addition, within this regime of relatively short surface cracks, micro-stress fields associated with surface roughness asperities are likely to have a significant influence on crack behaviour. As cracks extend deeper into material, the effect of asperity stresses diminishes but bulk Hertzian stresses become more important, which may potentially lead to a transition in crack behaviour and associated growth rates.

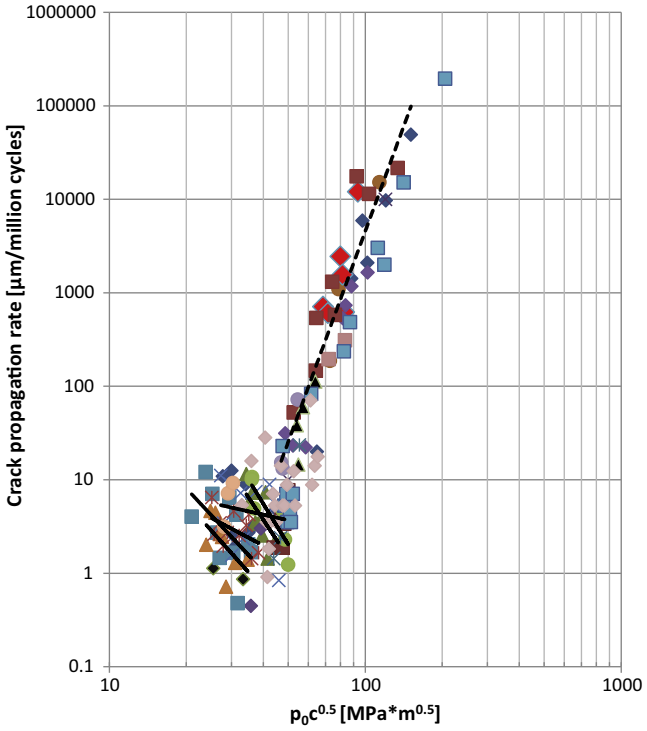

Fig. 15. Surface crack propagation rate as a function of parameter ($p_0 c^{0.5}$). Different markers represent individual cracks. Dotted trend line fitted to growth data of cracks longer than ~100 μm (i.e. cracks in stage 2 propagation identified earlier). Solid trend lines fitted to individual cracks shorter than ~100 μm (i.e. within stage 1 propagation). In total data for 22 cracks are shown.

5. Conclusions

Propagation of surface initiated cracks under rolling contact fatigue conditions was studied. Rolling contact fatigue tests were conducted on AISI 52100 bearing steel cylindrical roller specimens using a triple-contact test rig under mixed lubrication conditions. Surface cracks were detected early in life and their propagation across the surface monitored using a newly developed methodology. The main observations are:

- The observed crack morphology exhibited all the characteristics of typical RCF cracks found in engineering components and reported in literature, including v-shaped appearance at the surface, angle of inclination of 20–30° to the surface and propagation against the direction of friction force. In addition, crack branching, deflection, frequent crack arrests and secondary cracks reaching the surface were also observed.
- Crack growth from first detection to pitting was monitored and quantified under a range of contact pressures. Results show that the total life to pitting consists of crack initiation and propagation phases. Furthermore, crack growth measurements in elliptical contact tests under maximum Hertz pressure of 4.76 GPa show that most of the life, >80%, ***is consumed by the propagation phase under the contact conditions of mixed lubrication employed here.
- Direct evidence is provided of two distinct stages of crack propagation under rolling contact fatigue conditions: In stage 1, which, under conditions employed here, was associated with cracks up to about 100 μm in length, cracks show discontinuous growth with long periods of crack arrest. The average rate of crack growth was relatively low (~5–10 μm/million cycles) and decreased slightly with increasing crack length. This stage consumed most of the total life to pitting. In stage 2 propagation, reached once cracks exceeded the length of about 100 μm, propagation rate increases exponentially with crack length so that cracks extend much faster and eventually lead to pitting.
- A log-log plot of crack propagation rates against a product of the maximum contact pressure and square root crack length ($p_0c^{0.5}$), describing the applied stress intensity, produces a straight line for stage 2 cracks. Thus, the results provide first evidence that in the hereby-identified stage 2 propagation, growth of rolling contact fatigue cracks can be described by a Paris type propagation law, as commonly used in structural fatigue.

Acknowledgements

The authors would like to thank SKF Engineering and Research Centre, the Netherlands for providing financial support for this work.

References

[1] Tallian TE. On competing failure modes in rolling contact. ASLE Trans 1967;10(4):418–39.
[2] Soda N, Yamamoto T. Effect of tangential traction and roughness on crack initiation/propagation during rolling contact. ASLE Trans 1982;25(2):198–206.
[3] Borgese S. An electron fractographic study of spalls formed in rolling contact. J Basic Eng 1967;89(4):943.
[4] Martin JA, Eberhardt AD. Identification of potential failure nuclei in rolling contact fatigue. J Basic Eng 1967;89(4):932–42.
[5] Way S. Pitting due to rolling contact. J Appl Mech 1935;57:49–58.
[6] Nélias D, Dumont ML, Champiot F, Vincent A, Girodin D, Fougéres R, et al. Role of inclusions, surface roughness and operating conditions on rolling contact fatigue. J Tribol 1999;121(2):240–51.
[7] Onions RA, Archard JF. Pitting of gears and discs. Proc Inst Mech Eng Jun. 1974;188:673–82.
[8] Phillips MR, Quinn TFJ. The effect of surface roughness and lubricant film thickness on the contact fatigue life of steel surfaces lubricated with a sulphur-phosphorus type of extreme pressure additive. Wear 1978;51(1):11–24.
[9] Ueda T, Mitamura N. Mechanism of dent initiated flaking and bearing life enhancement technology under contaminated lubrication condition. Part II: effect of rolling element surface roughness on flaking resulting from dents, and life enhancement technology of rolling bearings. Tribol Int 2009;42(11–12):1832–7.
[10] Danner CH. Fatigue life of tapered roller bearings under minimal lubricant films. ASLE Trans 1970;13(4):241–51.
[11] Liu JY, Tallian TE, McCool JI. Dependence of bearing fatigue life on film thickness to surface roughness ratio. ASLE Trans 1975;18(2):144–52.
[12] Tallian TE, McCool JI, Sibley LB. Partial elastohydrodynamic lubrication in rolling contact. Proc Inst Mech Eng 1965;180:169–86.
[13] Soda N, Yamashita M, Osora K. Effect of tangential force on rolling contact fatigue. J JSLE 1971;16(8):573–84.
[14] Ueda T, Mitamura N. Mechanism of dent initiated flaking and bearing life enhancement technology under contaminated lubrication condition. Tribol Int Nov. 2008;41(11):965–74.
[15] Olver AV. The mechanism of rolling contact fatigue: an update. Proc Inst Mech Eng, Part J: J Eng Tribol 2005;219(5):313–30.
[16] Nakajima A, Ichimaru K, Hirano F. Effects of combination of rolling direction and sliding direction on pitting of rollers. J JSLE Int Ed 1983;4:93–8.
[17] Littmann W. The mechanism of contact fatigue. In: Interdisciplinary approach to the lubrication of concentrated contacts: Proceedings of a Symposium. p. 309–78.
[18] Lundberg G, Palmgren A. Dynamic capacity of rolling bearings. Acta Polytech Mech Eng Ser 1947;1(3):7.
[19] Ioannides E, Harris TA. A new fatigue life model for rolling bearings. J Tribol 1985;107(3):367.
[20] Sadeghi F, Jalalahmadi B, Slack TS, Raje N, Arakere NK. A review of rolling contact fatigue. J Tribol 2009;131(4):041403.
[21] Keer LM, Bryant MD, Haritos GK. Subsurface and surface cracking due to hertzian contact. J Lubr Technol 1982;104(3):347.
[22] Miller GR, Keer LM, Cheng HS. On the mechanics of fatigue crack growth due to contact loading. Proc Royal Soc A: Math, Phys Eng Sci 1985;397(1813):197–209.
[23] Murakami Y, Kaneta M, Yatsuzuka H. Analysis of surface crack propagation in lubricated rolling contact. ASLE Trans 1985;28(1):60–8.
[24] Kaneta M, Murakami Y. Effects of oil hydraulic pressure on surface crack growth in rolling/sliding contact. Tribol Int 1987;20(4):210–7.
[25] Kaneta M, Suetsugu M, Murakami Y. Mechanism of surface crack growth in lubricated rolling/sliding spherical contact. J Appl Mech 1986;53(2):354.
[26] Kaneta M, Murakami Y. Propagation of semi-elliptical surface cracks in lubricated rolling/sliding elliptical contacts. J Tribol 1991;113(2):270.
[27] Kaneta M, Yatsuzuka H, Murakami Y. Mechanism of crack growth in lubricated rolling/sliding contact. ASLE Trans 1985;28(3):407–14.
[28] Bower AF. The influence of crack face friction and trapped fluid on surface initiated rolling contact fatigue cracks. J Tribol 1988;110(4):704–11.
[29] Hanson MT, Keer LM. An analytical life prediction model for the crack propagation occurring in contact fatigue failure. Tribol Trans 1992;35(3):451–61.
[30] Murakami Y, Sakae C, Ichimaru K, Morita T. Experimental and fracture mechanics study of the pit formation mechanism under repeated lubricated rolling-sliding contact: effects of reversal of rotation and change of the driving roller. J Tribol 1997;119(4):788–96.
[31] Tyfour WR, Beynon JH. The effect of rolling direction reversal on fatigue crack morphology and propagation. Tribol Int Aug. 1994;27(4):273–82.
[32] Phillips MR, Chapman CJS. A magnetic method for detecting the onset of surface contact fatigue. Wear Aug. 1978;49(2):265–72.
[33] Wong SL, Bold PE, Brown MW, Allen RJ. Fatigue crack growth rates under sequential mixed-mode I and II loading cycles. Fatigue Fract Eng Mater Struct Aug. 2000;23(8):667–74.
[34] Suresh S. Fatigue crack deflection and fracture surface contact: micromechanical models. Metall Trans A 1985;16(1).
[35] Suresh S, Roberts TM. Propagation of short fatigue cracks. Int Metals Rev 1984;29(1):445–75.
[36] Lankford J. Initiation and early growth of fatigue cracks in high strength steel. Eng Fract Mech 1977;9(3):617–24.
[37] Yoshioka T, Fujiwara T. Measurement of propagation initiation and propagation time of rolling contact fatigue cracks by observation of acoustic emission and vibration. In: Proceedings of the 14th Leeds-Lyon Symposium on Tribology "Interface Dynamics", Lyon, France.
[38] Rahman MZ, Ohba H, Yoshioka T, Yamamoto T. Incipient damage detection and its propagation monitoring of rolling contact fatigue by acoustic emission. Tribol Int 2009;42(6):807–15.
[39] Rahman MZ, Ohba H, Yamamoto T, Yoshioka T. A study on incipient damage monitoring in rolling contact fatigue process using acoustic emission. Tribol Trans Sep. 2008;51(5):543–51.
[40] Miller K. The behaviour of short fatigue cracks and their initiation Part II - A general summary. Fatigue Fract Eng Mater Ellipsis 1987;10(2):93–113.